Article

Manufacturing of Carbon Nanotube-Polystyrene Filament for 3D Printing: Nanoparticle Dispersion and Electromagnetic Properties

Kseniya I. Baskakova [1,*], Alexander V. Okotrub [1,2], Lyubov G. Bulusheva [1,2] and Olga V. Sedelnikova [1,2,*]

1   Nikolaev Institute of Inorganic Chemistry, Siberian Branch of Russian Academy of Sciences, 630090 Novosibirsk, Russia
2   Radiophysics Department, National Research Tomsk State University, 634050 Tomsk, Russia
*   Correspondence: baskakova@niic.nsc.ru (K.I.B.); o.sedelnikova@gmail.com (O.V.S.)

Abstract: 3D printing is a promising technology for creating polymer objects of a given architecture with specified functional properties. In fact, the choice of filaments for 3D printing is quite limited. Here, we report a process for producing polystyrene filaments with 0.0025–2 wt.% single-walled carbon nanotubes (SWCNTs) by extruding crushed polystyrene composites. The resulting filaments are characterized by a high uniformity of filler distribution and the absence of air pores. Comparison of microscopy data and electromagnetic properties of base composites and composite materials printed from filaments showed that extrusion and printing improve SWCNT dispersion. The proposed method can be used to create filaments for 3D printing of objects from various base polymers containing functional fillers up to the electrical percolation threshold and above.

1. Introduction

The rapid and cost-effective manufacturing of physical objects with complex geometries and functional properties, tailored to a specific practical application, is one of the most challenging tasks in any process chain. The speed and precision of 3D printers make them a promising tool for prototyping polymer parts. Today, 3D printing is widely used in various fields, including electronics [1–3], optics [4–6], aerospace [7,8], and medicine [9,10]. Among other polymer-based 3D printing technologies [11–13], fused deposition modeling (FDM) looks the most promising for practical applications, including the production of capacitors [14,15], electromagnetic shielding components [16–18], sensors [19–21], and antistatic coatings [1,22]. FDM starts with the digital design of an element followed by the creation of a 3D object layer by layer from a polymer filament [2,23–26]. Although FDM printing is the most popular and economical method [27], it suffers from the limited choice of materials for 3D printing [28] and the associated narrow range of their physical characteristics. Thus, the development of a technique for manufacturing a 3D printing filament for the reproducible production of polymer objects with the required functional properties is an important issue for the industrial implementation of the FDM method.

The most common materials for 3D printing are thermoplastic elastomers such as polylactic acid (PLA), acrylonitrile butadiene styrene (ABS), polyurethane (PU), polyethylene (PE), and polystyrene (PS), etc., and less often, plastics with fillers are used [2,8,11,17,21,29,30]. Examples of the created products are a space radiation protection panels made of PE with the addition of basalt powder [8], a GHz frequency range screen made of PLA with 10% of graphene [17], and a tension sensor made of PU with carbon nanotubes (CNTs) [21]. A rather small number of works devoted to FDM printing from polymer filaments with nanoparticles is primarily due to the lack of commercially available materials for 3D printing and

preliminary studies of changes in the structure of the material during filament extrusion and subsequent 3D printing [28]. In addition, working with such materials is associated with the phenomenon of nanoparticle agglomeration, which worsens the functional properties of the created element [27,30] and can block the nozzle, causing material flow instability while printing [31].

On the other hand, methods for creating polymer composite (PC) films with nanoparticles are well-developed [32]. The exceptional structural and electronic transport properties of CNTs, combined with the highly adaptive characteristics of polymers, create a truly versatile platform for PC fabrication. In particular, the electrical conductivity and permittivity of PC strongly depend on the CNT content [33–36], demonstrating a critical behavior near the electrical percolation threshold. The percolation threshold can vary from 0.001 to 10 wt.% CNTs [37–46] depending on the type of polymer [37,47], properties of nanotubes [37], and their orientation [43,44]. However, dispersion of CNTs in the matrix seems to be the most significant for lowering the percolation threshold [43–46].

The problem of CNT aggregation can be solved by their functionalization [45,46], which is usually undesirable due to the deterioration of nanotube conductivity. Alternatively, these difficulties can be addressed by the right combination of homogenization techniques [41,43,48–50]. In particular, a higher level of CNT dispersion was obtained during post-treatment of PC on a forge-rolling machine [43]. Higher CNT dispersion lowers the percolation threshold, improving PC conductivity. Although forge-rolling reduces aggregates of nanoparticles, nanotubes are also destroyed at the same time [49,51]. Extrusion can also improve the dispersion of CNTs in a polymer but only if the solvent is completely evaporated before [50]. Otherwise, numerous air pores form in the volume of the extruded filament and the conductivity of the PC deteriorates [4,52].

In this work, we use homogenized PCs containing single-walled CNTs (SWCNTs) as the base material for filament extrusion for 3D printing instead of the traditional mixture of polymer and nanotubes. The proposed approach successfully works for a wide range of SWCNTs concentrations (0.0025–2 wt.%), improving the distribution of SWCNTs in PS matrix and lowering the electrical percolation threshold.

2. Materials and Methods

2.1. Materials

The material containing 75% SWCNTs with a diameter of 1.6–2.2 nm was produced by OCSiAl (Novosibirsk, Russia, LOT # 50-04122014). The catalyst and amorphous carbon by-products were removed according to the procedure described in [53]. SWCNTs (1 g) were heated in a muffle furnace at 500 °C for 1 h to open their tips and to oxidize amorphous carbon. The product was stirred in HCl (200 mL) for 12 h at 60 °C to dissolve the iron catalyst, washed with distilled water to neutral pH, and dried in a muffle furnace at 100 °C for 2 h. The content of amorphous carbon was less than 1% and the content of iron-containing particles did not exceed 2 wt.% [53]. The purified SWCNT sample consists of bundles of nanotubes with a diameter of about 20 nm and their agglomerates with a diameter of about 80–120 nm (see Supplementary Materials for details).

High-impact PS (HIPS-850) with a density of 1.04 g/cm^3 was used as the polymer base.

2.2. Filaments Preparation

Base PCs consisting of purified SWCNTs and PS were fabricated by the method described elsewhere [54]. PS granules (20 g), the required amount of SWCNTs, and CHCl$_3$ (300 mL) were treated with an ultrasonic homogenizer UZTA-0.15/22-O (U-SONIC, Biysk, Russia, 22 kHz) at a power of 70 W for 30 min. The resulting suspension was located in a fume hood at room temperature for a day and then in a desiccator at 40 °C until the solvent had completely evaporated.

The filaments were made from crushed base PCs with a SWCNT content of 0.0025–2 wt.% on a Wellzoom B single screw extruder (Shenzhen Mistar Technology Co., Ltd., Shenzhen, China) at a power of 120 W and a nozzle diameter of 2.85 mm. The extrusion temperatures varied from

195 to 235 °C depending on the viscosity of the composite, the screw speed was fixed to be about 100 rpm. The resulting filaments had the same diameter along the length, uniform color, and did not contain defects such as tears (see Supplementary Materials). That indicates that the polymer was not oxidized during extrusion and SWCNTs were evenly distributed throughout its volume.

It should be noted that filaments extruded from mechanical mixtures of PS and SWCNT powder [55,56] or PS and 10% SWCNT masterbatch [29,57–60] as starting materials demonstrated an extremely uneven nanotube distribution (see Supplementary Materials for details).

2.3. 3D Printing

3D printed samples were obtained from filaments on an Ultimaker 2 Go 3D printer (Ultimaker B.V., Amsterdam, the Netherlands). The printing temperature (210–260 °C) was selected experimentally for each SWCNT concentration, the platform temperature was about 90 °C, the printing speed was 30 mm/s, and printing was carried out with a 0.6 mm nozzle. The tolerance level of filament diameter was 2.85 ± 0.3 mm. Plates (12 × 12 × 0.6 mm) and rings (outer diameter 7.0 mm, inner diameter 3.0 mm, 2.3 mm) were printed. The upper temperature limit of the apparatus did not allow printing with a filament containing more than 0.5 wt.% SWCNTs due to clogging of a printer nozzle caused by the insufficient viscosity of the filled PC. The schematic representation of all stages of printed samples fabrication is shown in Figure 1.
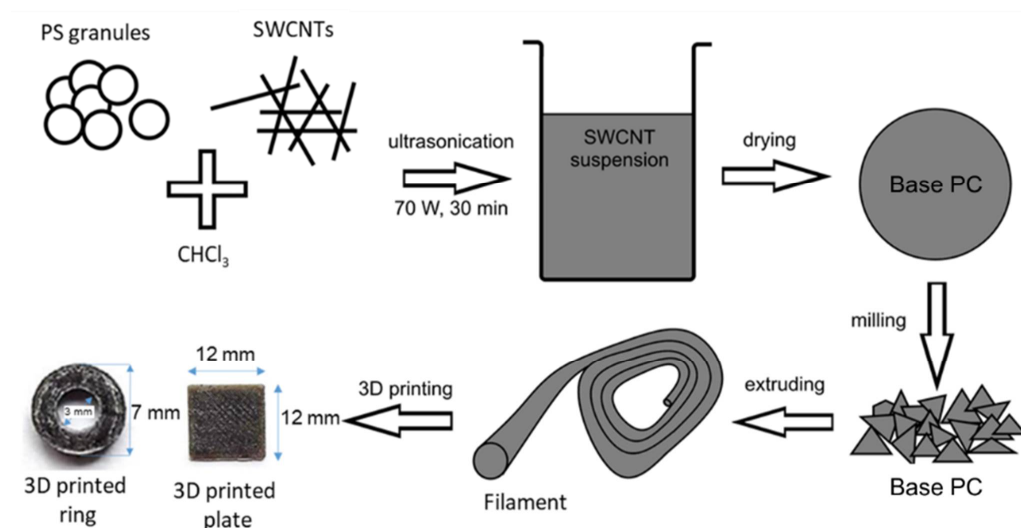
Figure 1. Scheme of the preparation of base composite materials, filaments, and 3D-printed samples from PS and SWCNTs.

2.4. Microscopic Characterization

The morphology of the base PCs with SWCNTs (films 200 μm thick), printed plates, and cross-sections of the obtained filaments was studied by optical microscopy using an Olympus BX51 microscope (Olimpus Corp., Tokyo, Japan) in transmission and reflection modes, respectively.

To examine the distribution of SWCNTs in PS in more details, the filaments with 0.005 and 0.1 wt.% filler loading were studied using scanning electron microscopy (SEM) on a JEOL-6700F microscope (JEOL Ltd., Tokyo, Japan) at an accelerating voltage of 15 kV. To do this, the filaments frozen with liquid nitrogen were broken perpendicular to their axes. The resulting cross-sections were covered with a 10 nm thick gold layer using a conventional sputtering tool.

2.5. Electromagnetic Measurements

The measurements were carried out for the base PC films and 3D printed samples (plates and rings). Plates were used to measure impedance at low frequencies, while rings were used to study GHz characteristics.

The real and imaginary components of the impedance were measured by the two-contact method on a Z-2000 impedance meter (Elins, Chernogolovka, Russia) in the frequency range of 1 kHz–2 MHz. The electrical conductivity σ_{AC} and permittivity ε_{AC} were reconstructed from the impedance data taking into account the following model [61]. The measurement cell was considered as four parallel elements: R_1 and C_1 are resistance and capacitance of the cell, and R_2 and C_2 are resistance and capacitance for studied PC film. R_1 and C_1 parameters were determined from the impedance data with empty cell while maintaining the same interplate distance as for the corresponding PC film. Further, the material parameters, namely the AC electrical conductivity σ_{AC} and permittivity ε_{AC}, were found from the calculated C_2 and R_2 values in assumption that the measurement cell can be considered as flat capacitor with leakage currents.

Microwave measurements were carried out on a Mikran P2M-04A scalar network analyzer (Mikran, Tomsk, Russia) in a coaxial cell 12.9 mm long in the range of 100 MHz–4 GHz using a voltage standing wave ratio (VSWR) sensor DK1-04-11R-11R (Mikran, Tomsk, Russia). As a result, the relative amplitudes of the wave reflected from the sample surface (S_{11}) and the wave transmitted through the sample (S_{21}) were obtained. The measured S-parameters were used to calculate the high-frequency values of ε_{AC} and σ_{AC} of the investigated materials in accordance with the referred works [62–64].

3. Results and Discussion

3.1. Optimization of Extrusion Conditions

The extrusion of PS granules without SWCNT additives was carried out at a temperature of 220 °C, which corresponds to the extrusion temperature of high-impact PS (190–230 °C). As a result, a uniform white filament with a diameter of 2.8 mm was obtained (Figure 2).
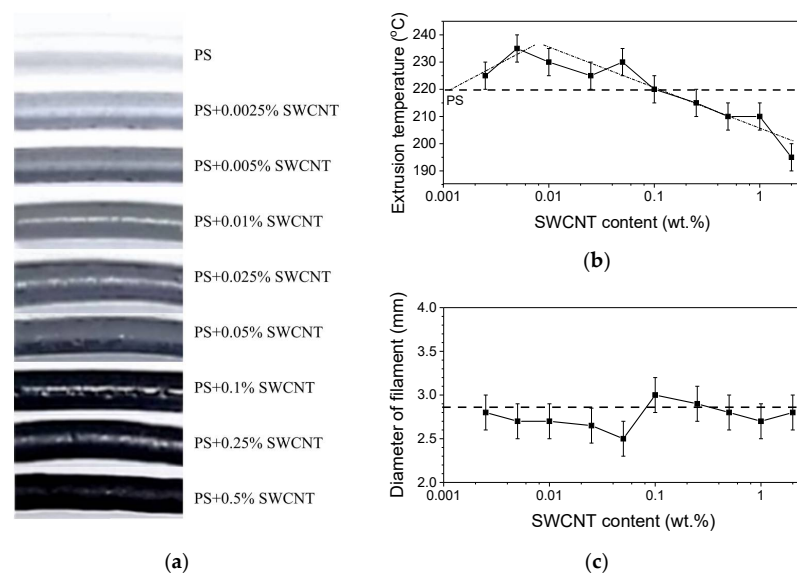
Figure 2. Images of PS filaments with different SWCNT concentrations (**a**), dependence of extrusion temperature (**b**), and diameter (**c**) of filament on SWCNT content.

The addition of SWCNTs affects the rheological properties of polymers [60,65]. The reorientation of nanotubes in the flow field during extrusion and the elimination of interpenetration of soft polymeric matrix with highly anisotropic nanoparticles change viscoelastic properties of melt matrix [65] and the plastic transition temperature [66]. As a result, the optimal extrusion temperature for obtaining filaments of an acceptable diameter (2.85 ± 0.3 mm)

varies depending on the nanotube content (Figure 2b,c). With increasing concentration from 0.0025 to 0.05 wt.%, the processing temperature becomes 5–20 °C higher than for clear PS. The maximum temperature of about 235 °C was required for the extrusion of PC with 0.005 wt.% SWCNTs. With a larger load of SWCNTs, the extrusion temperature decreases, reaching 195 °C for a filament with 2 wt.% SWCNTs. This behavior is associated with the high thermal conductivity coefficient for SWCNT bundles (6.6–126.6 W/(m K)) [67] versus 0.14 W/(m K) for PS [68]). Therefore, the heat released at the PS/SWCNT interface ensures the transition of the material to the plastic state at a lower temperature. It can be seen that the filament diameter decreases when SWCNTs are added to PS (Figure 2c). However, the dependence of the PC filament diameter on the SWCNT content shows a rise at a filler content of 0.1 wt.% followed by a gradual decrease. We assume that this indicates the formation of a network of nanotubes, which affects the flow of the polymer melt [65].

It should be noted that the reported temperatures are optimal for the PS filaments with SWCNTs at the screw speed of about 100 rpm using a Wellzoom B extruder. Changing any process parameter, while maintaining the found optimal temperature, will immediately affect the filament diameter.

3.2. Morphology of Base PCs and Filaments

Figure 3a,b shows transmission optical images of base PC films containing 0.005 and 0.1 wt.% SWCNTs. Even at lower nanotube concentrations, the base PC films appear opaque, however, areas of unfilled PS remain, indicating the formation of micron-sized SWCNT agglomerates, consistent with the previous work [69]. Cross-section images of filaments with the same SWCNT loading have a uniform black color without visible air pores and the unfilled areas of the polymer (Figure 3c,d). That distinguishes our filaments from those obtained in [4,52]. In the work [52], filaments were obtained using a mixture of ABS and multiwalled CNT solutions. The pores in those filaments were optically detected even after 8 extrusion cycles, while the electrical properties of the materials deteriorated after the third cycle. SEM analysis of fracture surfaces of filaments with SWCNT concentrations of 0.005 and 0.1 wt.% shows uniform nanotube networks coated with PS (Figure 3e,f). Bundles of nanotubes with a diameter of 15–20 nm and a length of about 2 μm can be distinguished (inset in Figure 3f). The better dispersion of SWCNTs in filaments as compared to base PCs could be explained by the splitting of SWCNT bundle agglomerates and improved distribution of nanotubes in the polymer matrix after extrusion.
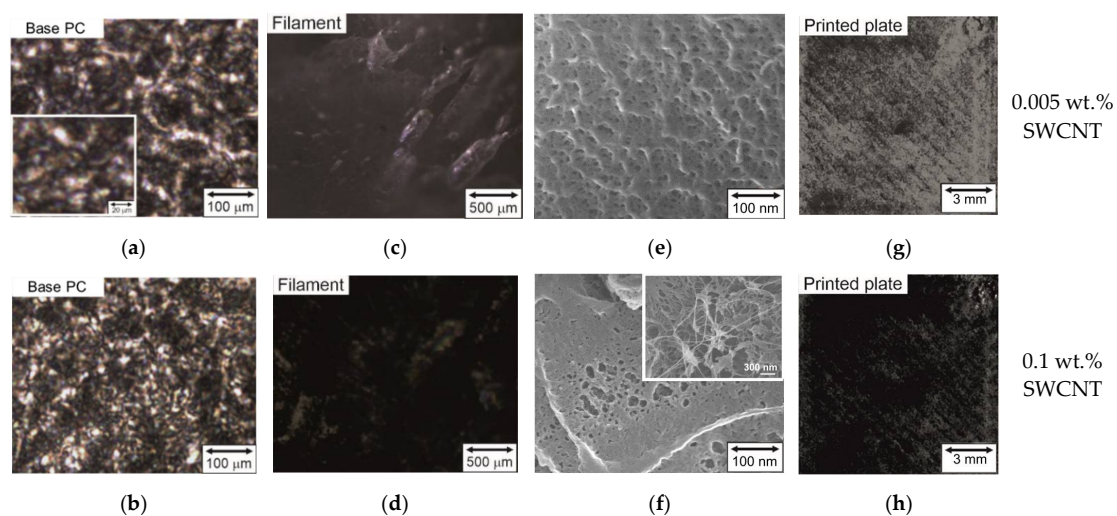
**Figure 3.** Microscopic study of PCs containing 0.005 wt.% SWCNTs (top images) and 0.1 wt.% SWCNTs (bottom images): optical images of base PC films (**a**,**b**), cross-sections of filaments (**c**,**d**), SEM images of filament cross-sections (**e**,**f**), and optical images of 3D printed plates (**g**,**h**). Inset in (**f**) shows SEM image of filament with 0.1 wt.% of SWCNTs from a region with poor SWCNT dispersion.

Figure 3g,h shows optical images of plates printed from the PC filaments with 0.005 and 0.1 wt.% SWCNTs. 3D printing was done crosswise in parallel lines at an angle of 45°. The surface roughness of the plates is related to the features of the method. The uniform color of the products indicates a uniform distribution of SWCNTs in PS.

3.3. Electrical Properties of Base PCs and Printed Samples

Figure 4 shows the frequency and concentration dependencies of AC electrical conductivity and permittivity for base PCs and plates printed from the filaments. At a frequency of 1 MHz, the AC conductivity of base PCs increases from 10^{-6} S/m to 10^{-5} S/m with an increase in the SWCNT content from 0.0025 to 0.5 wt.%. With a further increase in the nanotube loading, the increase in conductivity slows down (σ_{AC} is 10^{-4} S/m for base PC with 2.0 wt.% loading). This trend is less pronounced in microwaves (Figure 4c) due to the higher conductivities of both PS (black curves in Figure 4a,b) and SWCNTs [70]. The permittivity of base PCs at 1 MHz increases from 2.8 to 18.5 when the SWCNT loading changes from 0.025 to 0.5 wt.% (Figure 4d,f). A further increase in the SWCNT content reduces the permittivity, which drops to 4.2 at 2.0 wt.% SWCNTs. This phenomenon can be understood within the micro capacitor model [71]. At low loading, nanotubes and their bundles act as highly polarizable domains isolated from each other. The polymer layer separating adjacent nanoparticles becomes thinner with concentration, creating micro capacitors, causing a significant increase in permittivity, observed as a peak at 0.5 wt.% SWCNTs. Above this critical concentration, the thickness of the polymer decreases so much that the interparticle current increases the losses, deteriorating the permittivity to the value of the matrix.
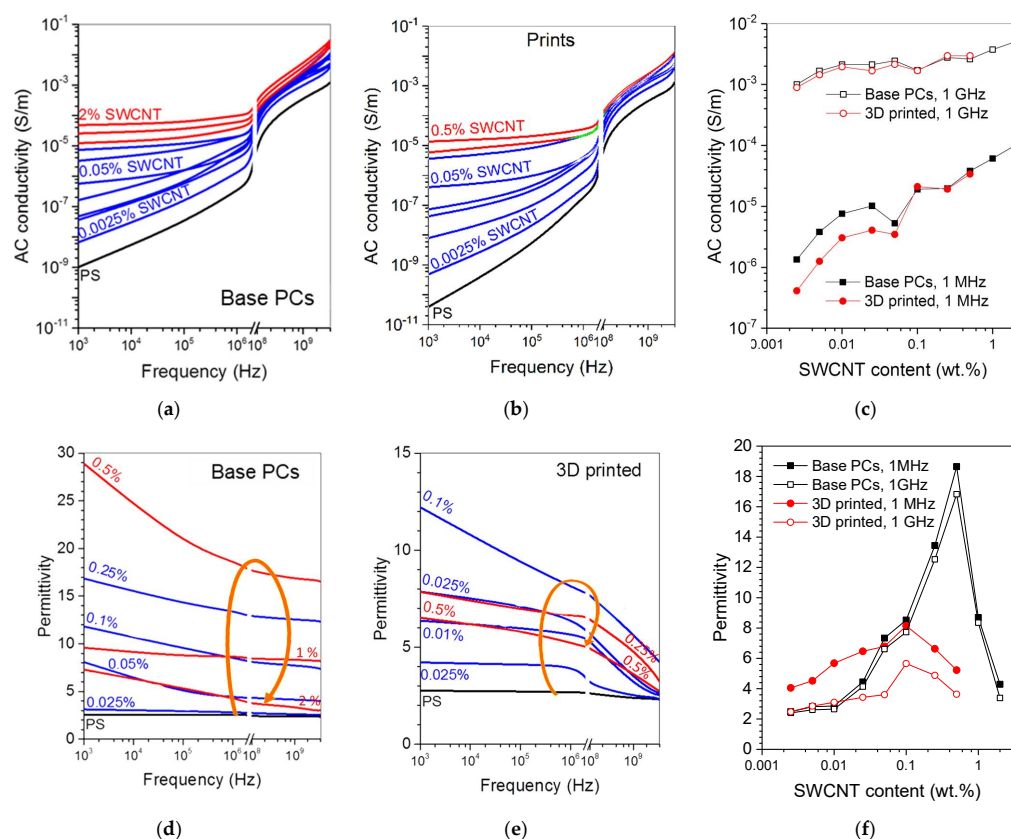
Figure 4. Frequency dependencies of AC conductivity and permittivity of base PC films (**a**,**d**) and printed samples (**b**,**e**). Concentration dependencies of the AC conductivity (**c**) and permittivity (**f**) of samples at 1 MHz and 1 GHz. Arrows in (**d**,**e**) follow the increase in SWCNT content.

At low concentrations of SWCNTs, the conductivity of printed samples somewhat decreases compared to the values for base PCs (Figure 4b,c). Transport degradation reflects changes in the network structure and composite architecture. SWCNTs are oriented in the flows of the extruder and printer [65], while nanotubes in base PCs are randomly distributed. Since the measurements are carried out for the in-plane orientation of the electric field relative to the PC layer, the conductivity of the printed plates is mainly characterized by the transverse conductivity of the nanotubes, while the response of the base PCs contains both less- and more-conductive components. On the other hand, microscopy images show that the surface of the printed plate is not flat (Figure 3g,h). This is due to the peculiarities of FDM technology. The product is grown layer by layer with several parallel print head passes. The deposited strips of diluted polymer cool down before the layer creation ends. The result is a relief surface. When the next polymer layer covers the previous one, the obtained air gaps go into volume of the printed product [11,72]. At a sufficiently high SWCNT concentration, these structural features do not affect the flow of electrical current through the sample. However, when the fraction of SWCNTs is small, inhomogeneity in the volume of the plate worsen its conductivity.

The maxima of the permittivity appeared in the printed plates at 0.1 wt.% SWCNTs (Figure 4e,f). Below this concentration, the permittivity of printed plates is higher than that of base PCMs containing the same SWCNT portion. This indicates that the extrusion and printing processes improve the dispersion of SWCNTs in PS as compared to base PCs.

Electromagnetic data show that highly conductive 3D printed composite materials can be used to create antistatic coatings and microwave screens.

4. Conclusions

Polymers with nanoparticles are in high demands for a range of practical applications such as flexible conductive screens, electromagnetic shielding, microwave and terahertz optics, etc. Each one requires materials with special properties formed to a certain architecture, which can be obtained using the modern technologies of 3D printing. In this work, we described a simple process for manufacturing of PS filaments with permittivity and conductivity determined by the SWCNT concentration for FDM 3D printer and evaluated the nanotube dispersion and electromagnetic properties of printed plates. The process is based on the extrusion of milled PCs and can be transferred to the production of highly homogeneous filaments from other thermoplastic polymer matrices and reinforcing materials. The absence of air pores in the filaments is achieved by careful evaporation of the solvent during the production of PC and optimization of extrusion parameters. Extrusion and 3D printing serve as additional steps for splitting the nanotube agglomerate inherited from base PCs and further improving the dispersion of SWCNTs. A comparison of the electromagnetic properties of base PCs and PCs printed from fabricated filaments revealed an improvement in the dielectric properties in the latter case. This suggests the practical application of the obtained material for 3D printing of protection skins for electronic components from damage caused by electrostatic discharge, impeding the output of any signal and preventing electromagnetic interference from affecting sensitive electronics.

Author Contributions: Conceptualization, A.V.O., L.G.B. and O.V.S.; Validation, A.V.O., L.G.B. and O.V.S.; Investigation, K.I.B.; Data curation, K.I.B.; Writing—original draft preparation, K.I.B.; Writing—review and editing K.I.B., L.G.B., O.V.S. and A.V.O.; Visualization, K.I.B.; Supervision, A.V.O. and O.V.S.; Project administration, O.V.S. and A.V.O.; Funding acquisition, A.V.O. All authors have read and agreed to the published version of the manuscript.

References

1. Zhang, L.; Du, W.; Nautiyal, A.; Liu, Z.; Zhang, X. Recent Progress on Nanostructured Conducting Polymers and Composites: Synthesis, Application and Future Aspects. *Sci. China Mater.* **2018**, *61*, 303–352. [CrossRef]
2. Stansbury, J.W.; Idacavage, M.J. 3D Printing with Polymers: Challenges among Expanding Options and Opportunities. *Dent. Mater.* **2016**, *32*, 54–64. [CrossRef] [PubMed]
3. Saleh Alghamdi, S.; John, S.; Roy Choudhury, N.; Dutta, N.K. Additive Manufacturing of Polymer Materials: Progress, Promise and Challenges. *Polymers* **2021**, *13*, 753. [CrossRef]
4. Wu, Y.; Isakov, D.; Grant, P. Fabrication of Composite Filaments with High Dielectric Permittivity for Fused Deposition 3D Printing. *Materials* **2017**, *10*, 1218. [CrossRef]
5. Jonušauskas, L.; Juodkazis, S.; Malinauskas, M. Optical 3D Printing: Bridging the Gaps in the Mesoscale. *J. Opt.* **2018**, *20*, 053001. [CrossRef]
6. Wang, H.; Wang, H.; Zhang, W.; Yang, J.K.W. Toward Near-Perfect Diffractive Optical Elements via Nanoscale 3D Printing. *ACS Nano* **2020**, *14*, 10452–10461. [CrossRef] [PubMed]
7. Kestilä, A.; Nordling, K.; Miikkulainen, V.; Kaipio, M.; Tikka, T.; Salmi, M.; Auer, A.; Leskelä, M.; Ritala, M. Towards Space-Grade 3D-Printed, ALD-Coated Small Satellite Propulsion Components for Fluidics. *Addit. Manuf.* **2018**, *22*, 31–37. [CrossRef]
8. Zaccardi, F.; Toto, E.; Santonicola, M.G.; Laurenzi, S. 3D Printing of Radiation Shielding Polyethylene Composites Filled with Martian Regolith Simulant Using Fused Filament Fabrication. *Acta Astronaut.* **2022**, *190*, 1–13. [CrossRef]
9. Sydney Gladman, A.; Garcia-Leiner, M.; Sauer-Budge, A.F. Emerging Polymeric Materials in Additive Manufacturing for Use in Biomedical Applications. *AIMS Bioeng.* **2019**, *6*, 1–20. [CrossRef]
10. Cresswell-Boyes, A.J.; Davis, G.R.; Krishnamoorthy, M.; Mills, D.; Barber, A.H. Composite 3D Printing of Biomimetic Human Teeth. *Sci. Rep.* **2022**, *12*, 7830. [CrossRef]
11. Saroia, J.; Wang, Y.; Wei, Q.; Lei, M.; Li, X.; Guo, Y.; Zhang, K. A Review on 3D Printed Matrix Polymer Composites: Its Potential and Future Challenges. *Int. J. Adv. Manuf. Technol.* **2020**, *106*, 1695–1721. [CrossRef]
12. Manoj Prabhakar, M.; Saravanan, A.K.; Haiter Lenin, A.; Jerin Leno, I.; Mayandi, K.; Sethu Ramalingam, P. A Short Review on 3D Printing Methods, Process Parameters and Materials. *Mater. Today Proc.* **2021**, *45*, 6108–6114. [CrossRef]
13. Kim, H.J.; Lim, S.W.; Lee, M.K.; Ju, S.W.; Park, S.H.; Ahn, J.S.; Hwang, K.G. Which Three-Dimensional Printing Technology Can Replace Conventional Manual Method of Manufacturing Oral Appliance? A Preliminary Comparative Study of Physical and Mechanical Properties. *Appl. Sci.* **2022**, *12*, 130. [CrossRef]
14. Yang, Y.; Chen, Z.; Song, X.; Zhu, B.; Hsiai, T.; Wu, P.-I.; Xiong, R.; Shi, J.; Chen, Y.; Zhou, Q.; et al. Three Dimensional Printing of High Dielectric Capacitor Using Projection Based Stereolithography Method. *Nano Energy* **2016**, *22*, 414–421. [CrossRef]
15. Hardin, J.O.; Grabowski, C.A.; Lucas, M.; Durstock, M.F.; Berrigan, J.D. All-Printed Multilayer High Voltage Capacitors with Integrated Processing Feedback. *Addit. Manuf.* **2019**, *27*, 327–333. [CrossRef]
16. Chizari, K.; Arjmand, M.; Liu, Z.; Sundararaj, U.; Therriault, D. Three-Dimensional Printing of Highly Conductive Polymer Nanocomposites for EMI Shielding Applications. *Mater. Today Commun.* **2017**, *11*, 112–118. [CrossRef]
17. Prashantha, K.; Roger, F. Multifunctional Properties of 3D Printed Poly(Lactic Acid)/Graphene Nanocomposites by Fused Deposition Modeling. *J. Macromol. Sci. Part A* **2017**, *54*, 24–29. [CrossRef]
18. Paddubskaya, A.; Valynets, N.; Kuzhir, P.; Batrakov, K.; Maksimenko, S.; Kotsilkova, R.; Velichkova, H.; Petrova, I.; Biró, I.; Kertész, K.; et al. Electromagnetic and Thermal Properties of Three-Dimensional Printed Multilayered Nano-Carbon/Poly(Lactic) Acid Structures. *J. Appl. Phys.* **2016**, *119*, 135102. [CrossRef]
19. Guo, S.Z.; Yang, X.; Heuzey, M.C.; Therriault, D. 3D Printing of a Multifunctional Nanocomposite Helical Liquid Sensor. *Nanoscale* **2015**, *7*, 6451–6456. [CrossRef]
20. Hauck, B.C.; Ruprecht, B.R.; Riley, P.C. Accurate and on-Demand Chemical Sensors: A Print-in-Place Ion Mobility Spectrometer. *Sens. Actuators B Chem.* **2022**, *362*, 131791. [CrossRef]
21. Vu, C.C.; Nguyen, T.T.; Kim, S.; Kim, J. Effects of 3D Printing-Line Directions for Stretchable Sensor Performances. *Materials* **2021**, *14*, 1791. [CrossRef] [PubMed]
22. Wu, C.S.; Liao, H.T. Interface Design of Environmentally Friendly Carbon Nanotube-Filled Polyester Composites: Fabrication, Characterisation, Functionality and Application. *Express Polym. Lett.* **2017**, *11*, 187–198. [CrossRef]
23. Berman, B. 3-D Printing: The New Industrial Revolution. *Bus. Horiz.* **2012**, *55*, 155–162. [CrossRef]
24. Zuo, Y.; Su, X.; Li, X.; Yao, Z.; Yu, T.; Zhou, J.; Li, J.; Lu, J.; Ding, J. Multimaterial 3D-Printing of Graphene/ $Li_{0.35}Zn_{0.3}Fe_{2.35}O_4$ and Graphene/Carbonyl Iron Composites with Superior Microwave Absorption Properties and Adjustable Bandwidth. *Carbon* **2020**, *167*, 62–74. [CrossRef]

25. Acquah, S.F.A.; Leonhardt, B.E.; Nowotarski, M.S.; Magi, J.M.; Chambliss, K.A.; Venzel, T.E.S.; Delekar, S.D.; Al-Hariri, L.A. Carbon Nanotubes and Graphene as Additives in 3D Printing. In *Carbon Nanotubes-Current Progress of Their Polymer Composites*; InTech: Vienna, Austria, 2016; pp. 227–251.

26. Fiedor, P.; Ortyl, J. A New Approach to Micromachining: High-Precision and Innovative Additive Manufacturing Solutions Based on Photopolymerization Technology. *Materials* **2020**, *13*, 2951. [CrossRef]

27. Joshi, A.; Goh, J.K.; Goh, K.E.J. Polymer-Based Conductive Composites for 3D and 4D Printing of Electrical Circuits. In *3D and 4D Printing of Polymer Nanocomposite Materials*; Elsevier: Amsterdam, The Netherlands, 2020; pp. 45–83. ISBN 9780128168059.

28. Sanatgar, R.H.; Cayla, A.; Campagne, C.; Nierstrasz, V. Morphological and Electrical Characterization of Conductive Polylactic Acid Based Nanocomposite before and after FDM 3D Printing. *J. Appl. Polym. Sci.* **2019**, *136*, 47040. [CrossRef]

29. Shemelya, C.; De La Rosa, A.; Torrado, A.R.; Yu, K.; Domanowski, J.; Bonacuse, P.J.; Martin, R.E.; Juhasz, M.; Hurwitz, F.; Wicker, R.B.; et al. Anisotropy of Thermal Conductivity in 3D Printed Polymer Matrix Composites for Space Based Cube Satellites. *Addit. Manuf.* **2017**, *16*, 186–196. [CrossRef]

30. Shah, S.; Shiblee, M.N.I.; Rahman, J.M.H.; Basher, S.; Mir, S.H.; Kawakami, M.; Furukawa, H.; Khosla, A. 3D Printing of Electrically Conductive Hybrid Organic–Inorganic Composite Materials. *Microsyst. Technol.* **2018**, *24*, 4341–4345. [CrossRef]

31. Gnanasekaran, K.; Heijmans, T.; van Bennekom, S.; Woldhuis, H.; Wijnia, S.; de With, G.; Friedrich, H. 3D Printing of CNT- and Graphene-Based Conductive Polymer Nanocomposites by Fused Deposition Modeling. *Appl. Mater. Today* **2017**, *9*, 21–28. [CrossRef]

32. Parvej, M.S.; Khan, M.I.; Hossain, M.K. Preparation of Nanoparticle-Based Polymer Composites. In *Nanoparticle-Based Polymer Composites*; Elsevier: Amsterdam, The Netherlands, 2022; pp. 55–94.

33. Sankaran, S.; Deshmukh, K.; Ahamed, M.B.; Khadheer Pasha, S.K. Recent Advances in Electromagnetic Interference Shielding Properties of Metal and Carbon Filler Reinforced Flexible Polymer Composites: A Review. *Compos. Part A Appl. Sci. Manuf.* **2018**, *114*, 49–71. [CrossRef]

34. Thomassin, J.M.; Jérôme, C.; Pardoen, T.; Bailly, C.; Huynen, I.; Detrembleur, C. Polymer/Carbon Based Composites as Electromagnetic Interference (EMI) Shielding Materials. *Mater. Sci. Eng. R Rep.* **2013**, *74*, 211–232. [CrossRef]

35. Bychanok, D.S.; Shuba, M.V.; Kuzhir, P.P.; Maksimenko, S.A.; Kubarev, V.V.; Kanygin, M.A.; Sedelnikova, O.V.; Bulusheva, L.G.; Okotrub, A.V. Anisotropic Electromagnetic Properties of Polymer Composites Containing Oriented Multiwall Carbon Nanotubes in Respect to Terahertz Polarizer Applications. *J. Appl. Phys.* **2013**, *114*, 114304. [CrossRef]

36. Okotrub, A.V.; Yudanov, N.F.; Aleksashin, V.M.; Bulusheva, L.G.; Komarova, O.A.; Kostas, U.O.; Gevko, P.N.; Antyufeeva, N.V.; Il'chenko, S.I.; Gunyaev, G.M. Study of Thermal and Mechanical Properties of Composites Based on Arc-Grown Carbon Nanotubes and Heat-Resistant Cyanoether Binder. *Polym. Sci. Ser. A* **2007**, *49*, 702–707. [CrossRef]

37. Larionov, S.A.; Deev, I.S.; Petrova, G.N.; Bader, E.Y. Influence of Carbon Fillers on Electrophysical, Mechanical and Rheological Properties of Polyethylene. *Proc. VIAM* **2013**, *9*, 1–10.

38. Klyuev, I.Y.; Shevchenko, V.G.; Kuperman, A.M.; Solodilov, V.I. Electrophysical Characteristics of Epoxy Nanocomposites with Ultralow Percolation Thresholds. *Inorg. Mater. Appl. Res.* **2020**, *11*, 416–419. [CrossRef]

39. Yan, Y.; Cui, J.; Zhao, S.; Zhang, J.; Liu, J.; Cheng, J. Interface Molecular Engineering of Single-Walled Carbon Nanotube/Epoxy Composites. *J. Mater. Chem.* **2012**, *22*, 1928–1936. [CrossRef]

40. Hoseini, A.H.A.; Arjmand, M.; Sundararaj, U.; Trifkovic, M. Significance of Interfacial Interaction and Agglomerates on Electrical Properties of Polymer-Carbon Nanotube Nanocomposites. *Mater. Des.* **2017**, *125*, 126–134. [CrossRef]

41. Kausar, A.; Ahmad, S.; Salman, S.M. Effectiveness of Polystyrene/Carbon Nanotube Composite in Electromagnetic Interference Shielding Materials: A Review. *Polym. Plast. Technol. Eng.* **2017**, *56*, 1027–1042. [CrossRef]

42. Ayewah, D.O.O.; Davis, D.C.; Krishnamoorti, R.; Lagoudas, D.C.; Sue, H.-J.; Willson, M. A Surfactant Dispersed SWCNT-Polystyrene Composite Characterized for Electrical and Mechanical Properties. *Compos. Part A Appl. Sci. Manuf.* **2010**, *41*, 842–849. [CrossRef]

43. Sedelnikova, O.V.; Kanygin, M.A.; Korovin, E.Y.; Bulusheva, L.G.; Suslyaev, V.I.; Okotrub, A.V. Effect of Fabrication Method on the Structure and Electromagnetic Response of Carbon Nanotube/Polystyrene Composites in Low-Frequency and Ka Bands. *Compos. Sci. Technol.* **2014**, *102*, 59–64. [CrossRef]

44. Spitalsky, Z.; Tasis, D.; Papagelis, K.; Galiotis, C. Carbon Nanotube-Polymer Composites: Chemistry, Processing, Mechanical and Electrical Properties. *Prog. Polym. Sci.* **2010**, *35*, 357–401. [CrossRef]

45. Guo, B.; Ji, X.; Chen, X.; Li, G.; Lu, Y.; Bai, J. A Highly Stretchable and Intrinsically Self-Healing Strain Sensor Produced by 3D Printing. *Virtual Phys. Prototyp.* **2020**, *15*, 520–531. [CrossRef]

46. Zhang, A.; Luan, J.; Zheng, Y.; Sun, L.; Tang, M. Effect of Percolation on the Electrical Conductivity of Amino Molecules Non-Covalently Coated Multi-Walled Carbon Nanotubes/Epoxy Composites. *Appl. Surf. Sci.* **2012**, *258*, 8492–8497. [CrossRef]

47. Watt, M.R.; Gerhardt, R.A. Factors That Affect Network Formation in Carbon Nanotube Composites and Their Resultant Electrical Properties. *J. Compos. Sci.* **2020**, *4*, 100. [CrossRef]

48. Grossiord, N.; Loos, J.; Van Laake, L.; Maugey, M.; Zakri, C.; Koning, C.E.; John Hart, A. High-Conductivity Polymer Nanocomposites Obtained by Tailoring the Characteristics of Carbon Nanotube Fillers. *Adv. Funct. Mater.* **2008**, *18*, 3226–3234. [CrossRef]

49. Kanygin, M.A.; Sedelnikova, O.V.; Bulusheva, L.G.; Okotrub, A.V. Polymer-Assisted Forge-Rolling Disaggregation of Detonation Nanodiamonds and Onion-like Carbon. *Int. J. Nanotechnol.* **2015**, *12*, 182. [CrossRef]

50. Mahfuz, H.; Khan, M.R.; Leventouri, T.; Liarokapis, E. Investigation of MWCNT Reinforcement on the Strain Hardening Behavior of Ultrahigh Molecular Weight Polyethylene. *J. Nanotechnol.* **2011**, *2011*, 1–9. [CrossRef]

51. Kanygin, M.A.; Sedelnikova, O.V.; Asanov, I.P.; Bulusheva, L.G.; Okotrub, A.V.; Kuzhir, P.P.; Plyushch, A.O.; Maksimenko, S.A.; Lapko, K.N.; Sokol, A.A.; et al. Effect of Nitrogen Doping on the Electromagnetic Properties of Carbon Nanotube-Based Composites. *J. Appl. Phys.* **2013**, *113*, 144315. [CrossRef]

52. Smygalina, P.P.; Trofimov, E.A.; Pidotova, D.A.; Badin, A.V. Evaluation of the Effect of Porosity of Composite ABS Filament with MWCNTs on Its Electrophysical Properties in the EHF Range. In Proceedings of the Sixteenth All-Russian Conference of Student Research Incubators, Tomsk, Russia, 13–15 May 2019; pp. 69–72.

53. Gurova, O.A.; Arhipov, V.E.; Koroteev, V.O.; Guselnikova, T.Y.; Asanov, I.P.; Sedelnikova, O.V.; Okotrub, A.V. Purification of Single-Walled Carbon Nanotubes Using Acid Treatment and Magnetic Separation. *Phys. Status Solidi B* **2019**, *256*, 1800742. [CrossRef]

54. Sedelnikova, O.V.; Baskakova, K.I.; Gusel'nikov, A.V.; Plyusnin, P.E.; Bulusheva, L.G.; Okotrub, A.V. Percolative Composites with Carbon Nanohorns: Low-Frequency and Ultra-High Frequency Response. *Materials* **2019**, *12*, 1848. [CrossRef]

55. Dastjerdi, R.; Mojtahedi, M.R.M.; Shoshtari, A.M. Comparing the Effect of Three Processing Methods for Modification of Filament Yarns with Inorganic Nanocomposite Filler and Their Bioactivity against Staphylococcus Aureus. *Macromol. Res.* **2009**, *17*, 378–387. [CrossRef]

56. Liu, Z.; Tu, R.; Liao, Q.; Hu, H.; Yang, J.; He, Y.; Bian, H.; Ma, L.; Liu, W. High Thermal Conductivity of Flake Graphite Reinforced Polyethylene Composites Fabricated by the Powder Mixing Method and the Melt-Extruding Process. *Polymers* **2018**, *10*, 693. [CrossRef]

57. Spinelli, G.; Lamberti, P.; Tucci, V.; Kotsilkova, R.; Ivanov, E.; Menseidov, D.; Naddeo, C.; Romano, V.; Guadagno, L.; Adami, R.; et al. Nanocarbon/Poly(Lactic) Acid for 3D Printing: Effect of Fillers Content on Electromagnetic and Thermal Properties. *Materials* **2019**, *12*, 2369. [CrossRef]

58. Dorigato, A.; Moretti, V.; Dul, S.; Unterberger, S.H.; Pegoretti, A. Electrically Conductive Nanocomposites for Fused Deposition Modelling. *Synth. Met.* **2017**, *226*, 7–14. [CrossRef]

59. Oseli, A.; Vesel, A.; Mozetič, M.; Žagar, E.; Huskić, M.; Slemenik Perše, L. Nano-Mesh Superstructure in Single-Walled Carbon Nanotube/Polyethylene Nanocomposites, and Its Impact on Rheological, Thermal and Mechanical Properties. *Compos. Part A Appl. Sci. Manuf.* **2020**, *136*, 105972. [CrossRef]

60. Mitchell, C.A.; Bahr, J.L.; Arepalli, S.; Tour, J.M.; Krishnamoorti, R. Dispersion of Functionalized Carbon Nanotubes in Polystyrene. *Macromolecules* **2002**, *35*, 8825–8830. [CrossRef]

61. Gavrilov, N.N.; Okotrub, A.V.; Bulusheva, L.G.; Sedelnikova, O.V.; Yushina, I.V.; Kuznetsov, V.L. Dielectric Properties of Polystyrene/Onion-like Carbon Composites in Frequency Range of 0.5–500 kHz. *Compos. Sci. Technol.* **2010**, *70*, 719–724. [CrossRef]

62. Nicolson, A.M.; Ross, G.F. Measurement of the Intrinsic Properties of Materials by Time-Domain Techniques. *IEEE Trans. Instrum. Meas.* **1970**, *19*, 377–382. [CrossRef]

63. Weir, W.B. Automatic Measurement of Complex Dielectric Constant and Permeability. *Proc. IEEE* **1974**, *62*, 33–36. [CrossRef]

64. EM-Calculator, Online Calculator of Complex Dielectric Permittivity and Magnetic Permeability in Microwaves. 2022. Available online: http://em-calculator.com (accessed on 1 September 2022).

65. Kharchenko, S.B.; Douglas, J.F.; Obrzut, J.; Grulke, E.A.; Migler, K.B. Flow-Induced Properties of Nanotube-Filled Polymer Materials. *Nat. Mater.* **2004**, *3*, 564–568. [CrossRef]

66. Grady, B.P.; Paul, A.; Peters, J.E.; Ford, W.T. Glass Transition Behavior of Single-Walled Carbon Nanotube-Polystyrene Composites. *Macromolecules* **2009**, *42*, 6152–6158. [CrossRef]

67. Hou, J.; Wang, X.; Vellelacheruvu, P.; Guo, J.; Liu, C.; Cheng, H.-M. Thermal Characterization of Single-Wall Carbon Nanotube Bundles Using the Self-Heating 3ω Technique. *J. Appl. Phys.* **2006**, *100*, 124314. [CrossRef]

68. T'Joen, C.; Park, Y.; Wang, Q.; Sommers, A.; Han, X.; Jacobi, A. A Review on Polymer Heat Exchangers for HVAC&R Applications. *Int. J. Refrig.* **2009**, *32*, 763–779. [CrossRef]

69. Yan, Y.; Cui, J.; Pötschke, P.; Voit, B. Dispersion of Pristine Single-Walled Carbon Nanotubes Using Pyrene-Capped Polystyrene and Its Application for Preparation of Polystyrene Matrix Composites. *Carbon* **2010**, *48*, 2603–2612. [CrossRef]

70. Shuba, M.V.; Yuko, D.I.; Gorokhov, G.; Meisak, D.; Bychanok, D.S.; Kuzhir, P.P.; Maksimenko, S.A.; Angelova, P.; Ivanov, E.; Kotsilkova, R. Frequency and Density Dependencies of the Electromagnetic Parameters of Carbon Nanotube and Graphene Nanoplatelet Based Composites in the Microwave and Terahertz Ranges. *Mater. Res. Express* **2019**, *6*, 095050. [CrossRef]

71. Yuan, J. Percolation of Carbon Nanomaterials for High-k Polymer Nanocomposites. *Chin. Chem. Lett.* **2017**, *28*, 2036–2044. [CrossRef]

72. Riddick, J.C.; Haile, M.A.; Von Wahlde, R.; Cole, D.P.; Bamiduro, O.; Johnson, T.E. Fractographic Analysis of Tensile Failure of Acrylonitrile-Butadiene-Styrene Fabricated by Fused Deposition Modeling. *Addit. Manuf.* **2016**, *11*, 49–59. [CrossRef]